Dyes and Pigments 91 (2011) 317–323

Contents lists available at ScienceDirect

Dyes and Pigments

journal homepage: www.elsevier.com/locate/dyepig

Electronically coupled porphyrin-arene dyads for dye-sensitized solar cells

Cheng-Wei Lee [a,b], Hsueh-Pei Lu [b], Nagannagari Masi Reddy [a], Hsuan-Wei Lee [a], Eric Wei-Guang Diau [b,*], Chen-Yu Yeh [a,*]

[a] Department of Chemistry, National Chung Hsing University, Taichung 402, Taiwan, ROC
[b] Department of Applied Chemistry and Institute of Molecular Science, National Chiao Tung University, Hsinchu 300, Taiwan, ROC

ARTICLE INFO

Article history:
Received 15 February 2011
Received in revised form
7 April 2011
Accepted 7 April 2011
Available online 21 April 2011

Keywords:
π-Conjugation
Dye-sensitized solar cells
Electronic coupling
Light-harvesting
Perylenes
Porphyrins

ABSTRACT

An acetylene-linked porphyrin-perylene anhydride and an acetylene-linked porphyrin-naphthalic anhydride have been synthesized; the highly conjugated acetylenic bridge in these porpyrins efficiently mediates electronic interaction between the porphyrin and perylene units to extend the π-conjugation of the porphyrin dye and to cause both broadening and red shifts of both the Soret and Q absorption bands. This condition is a useful feature for efficient dye-sensitized solar cell applications. The optical, electrochemical and photovoltaic properties of the new linked anhydrides show that the HOMO–LUMO gap decreased upon extension of π-conjugation, indicating a strong electronic coupling between the porphyrin and the perylene or naphthalene unit.

1. Introduction

To maintain global economic growth and to diminish global warming and environmental pollution, the exploration of renewable energy resources is of great significance. Sunlight is the most abundant resource that can deliver clean and efficient energy to meet the increasing demand worldwide. Nature has chosen porphyrin-related pigments in the light-harvesting antennae of photosynthetic organisms that power biological systems [1]. The chromophores in the photosynthetic reaction center capture sunlight efficiently and convert solar energy into usable chemical energy. The synthesis of porphyrins and related macrocycles has attracted considerable attention because they are ubiquitous in natural systems and have prospective applications in mimicking enzymes [2], catalytic reactions [3], photodynamic therapy [4], molecular electronic devices and conversion of solar energy [5–15]. In particular, numerous porphyrin-based artificial light-harvesting antennae, and donor–acceptor dyads and triads have been prepared and tested to improve our understanding of the photochemical aspect of natural photosynthesis [5–15]. Extensive investigation on these multicomponent systems has disclosed the reaction parameters and the mechanism of transfer of energy and electrons have illuminated the development of the conversion of solar energy.

The development of solar cells of new types is escalating, prompted by increasing energy demand. Dye-sensitized solar cells (DSSC) appear to be a promising approach for the conversion of sunlight to electricity on a large scale. The most efficient DSSC are based on ruthenium polypyridine complexes and have attained efficiencies ~11% of power conversion [16,17]. However, the application of ruthenium complex devices is significantly limited by the rareness of ruthenium and also by potential environmental pollution issues. Diverse organic dyes including porphyrin-related compounds have consequently been synthesized for use in DSSC [5–15]. Officer et al. have synthesized β-carboxyl-substituted porphyrin monomers and multiporphyrin arrays, and investigated their efficiencies [18]; β-substituted monoporphyrin carboxylic-acid derivatives with a conjugated bridge are effective candidates for DSSC. The best porphyrin dye, which has a butadiene bridge between a carboxyl and the porphyrin ring, attains an efficiency up to 7.1% in its power conversion [10]. The conjugated bridge significantly broadens the absorption bands to increase the light-harvesting ability. To increase the absorption width of a porphyrin, Imahori et al. designed and synthesized a naphthyl-fused porphyrin with elongated π-conjugation. The cell performance of the naphthyl-fused porphyrin is improved by about 50% relative to the non-fused porphyrin derivative [19].

* Corresponding authors. Fax: +886 4 22862547.
E-mail addresses: diau@mail.nctu.edu.tw (E.W.-G. Diau), cyyeh@dragon.nchu.edu.tw (C.-Y. Yeh).

0143-7208/$ – see front matter © 2011 Elsevier Ltd. All rights reserved.
doi:10.1016/j.dyepig.2011.04.010

Similar to porphyrin derivatives, perylenes are attractive molecular components for application in molecular electronic devices because of their great photostability and unique structures, and their electrochemical and photophysical properties [20–23]. Several perylene dyes for DSSC have been rationally designed and synthesized with introduction of electron-donating groups and bulky substituents to decrease aggregation. The most effective perylene dyes show a power conversion efficiency of up to 6.8% [24,25].

On the basis of previous work, extension of π-conjugation of the porphyrin dye appears to cause broadening of the absorption bands, which is an essential requirement for an efficient sensitizer [5–15,18,19]. We thus aim to construct electronically coupled porphyrin-arene dyads as sensitizers for use in DSSC. Here, we report the synthesis of porphyrin-perylene anhydride dyad **4** and porphyrin- naphthalene anhydride dyad **5**, and their optical, electrochemical and photovoltaic properties. A perylene sensitizer (**P1**) was also synthesized for comparison.

2. Experimental

All reagents and solvents were obtained from commercial sources and used without further purification, unless otherwise noted. CH_2Cl_2 was dried over CaH_2 and freshly distilled before use. THF was dried over sodium/benzophenone and freshly distilled before use. Tetrabutylammonium hexafluorophosphate ($TBAPF_6$) was recrystallized twice from absolute ethanol and further dried for two days under vacuum. Column chromatography was performed on silica gel (Merck, 70–230 Mesh ASTM).

2.1. Spectral and electrochemical measurements

^{1}H NMR spectra (Varian spectrometer, 400 MHz), UV–visible spectra (Varian Cary 50), UV–visible–NIR spectra (Shimadzu UV-3600), emission spectra (JASCO FP-6000 spectrofluorimeter), High resolution mass spectra (LTQ Orbitrap XL, Thermo Fisher Scientific) and FAB mass spectra (JMS-SX/SX102A Tandem Mass spectrometer) were recorded on the indicated instruments. Electrochemical tests were performed with a three-electrode potentiostat (CH Instruments, Model 750A) in THF deoxygenated on purging with pre-purified dinitrogen gas. Cyclic voltammetry was conducted with a three-electrode cell equipped with a BAS glassy carbon disk (0.07 cm^2) as the working electrode, a platinum wire as auxiliary electrode, and an Ag/AgCl (saturated) reference electrode; the reference electrode is separated from the bulk solution with a double junction filled with electrolyte solution. The working electrode was polished with aluminium (0.03 μm) on felt pads (Buehler) and treated ultrasonically for 1 min before each experiment. The reproducibility of individual potential values was within ±5 mV.

2.2. Device fabrication

The porphyrins were sensitized onto TiO_2 nanoparticulate films to serve as working electrodes in DSSC devices. A paste composed of TiO_2 particles (~20 nm) for the transparent active layer was coated on a $TiCl_4$-treated FTO glass substrate (FTO, 8 Ω/cm^{-2}) with repetitive screen printing to obtain the required film thickness (~10 μm). The TiO_2 film was annealed according to a programmed procedure: (1) heating at 80 °C for 15 min; (2) heating at 135 °C for 10 min; (3) heating at 325 °C for 30 min; (4) heating at 375 °C for 5 min; (5) heating at 450 °C for 15 min; (6) heating at 500 °C for 15 min. For each dye **P1**, **4** and **5**, the electrode was immersed in the dry DMF solution (0.2 mM, 25 °C) containing tetrabutylammonium hydroxide (TBA, 0.2 mM) for dye loading onto the TiO_2 film at 25 °C for 4 h and 8 h. The Pt counter electrodes were prepared on spin-coating drops of H_2PtCl_6 solution onto ITO glass and heating at 380 °C for 15 min. To prevent a short circuit, the two electrodes were assembled into a cell of sandwich type and sealed with a hot-melt film (SX1170, Solaronix, thickness 25 μm). The electrolyte solution containing LiI (0.1 M), I_2 (0.05 M), PMII (0.6 M), 4-*tert*-butylpyridine (0.5 M) in a mixture of acetonitrile and valeronitrile (volume ratio 1:1) was introduced into the space between the two electrodes, so completing the fabrication of these DSSC devices.

2.3. Photovoltaic characterization

The current-voltage characteristics of the devices were measured with a solar simulator (AM 1.5, SAN-EI, XES-502S, type class A) calibrated with a Si-based reference cell (VLSI standards, Oriel PN 91150V). When the device is irradiated with the solar simulator, the source meter (Keithley 2400, computer-controlled) sends a voltage (V) to the device, and the photocurrent (I) is read at each step controlled by a computer via a GPIB interface. The efficiency (η) of conversion of light to electricity is obtained with this relation, $\eta = J_{sc}\, V_{oc}\, FF/P_{in}$, in which J_{sc} (mA cm^{-2}) is the current density measured at short circuit, and V_{oc} (V) is the voltage measured at open circuit. P_{in} is the input radiation power (for one-sun illumination $P_{in} = 100$ mW cm^{-2}) and FF is the filling factor. The incident monochromatic efficiency for conversion from photons to current (IPCE) spectra of the corresponding devices was measured with a system comprising a Xe lamp (PTi A-1010, 150 W), monochromator (Dongwoo DM150i, 1200 g/mm blazed at 500 nm), and source meter (Keithley 2400, computer-controlled). A standard Si photodiode (ThorLabs FDS1010) served as a reference to calibrate the power density of the light source at each wavelength. Photocurrent densities of both the target device and the reference Si cell were measured under the same experimental conditions (excitation beam size ~0.08 cm^2) so to obtain the IPCE value of the device from comparison of the current ratio and the value of the reference cell at each wavelength.

2.4. Synthesis of dyes *4*, *5*, and *P1*

2.4.1. Zinc(II) 5,15-Bis(3,5-di-tert-butylphenyl)-10-(bis(4-octylphenyl)amino)-20-(3- (perylenedicarboxylic-9,10-anhydride) ethynyl)porphyrin (*4*)

To a solution of porphyrin **2** [5] (26.4 mg, 0.02 mmol) in dry THF (5 mL) was added tetrabutylammonium fluoride (TBAF) 1 M in THF (0.08 mL, 0.08 mmol). The solution was stirred at 25 °C for 30 min under dinitrogen. The mixture was quenched with H_2O and then extracted with CH_2Cl_2. The organic layer was dried over anhydrous Na_2SO_4 and the solvent was removed under vacuum. The residue and 9-bromo-perylene-3,4-dicarboxylic anhydride (16.0 mg, 0.04 mmol) were dissolved in dry THF (5 mL) and NEt_3 (1 mL) and degassed with dinitrogen for 10 min; then $Pd_2(dba)_3$ (2.2 mg, 2.5 μmol) and $AsPh_3$ (6 mg, 0.02 mmol) were added to the mixture. The solution was heated under reflux for 3 h under dinitrogen. The solvent was removed under vacuum. The residue was purified on a column chromatograph (silica gel) using CH_2Cl_2/hexane = 4/6 as eluent. Recrystallization from CH_2Cl_2/CH_3OH gave **4** (13.4 mg, 45%). ^{1}H NMR ($CDCl_3$, 400 MHz) δ 9.49 (d, J = 4.4 Hz, 2H), 9.22 (d, J = 4.8 Hz, 2H), 9.00 (d, J = 8.0 Hz, 1H), 8.94 (d, J = 4.4 Hz, 2H), 8.77 (d, J = 4.8 Hz, 2H), 8.42–8.36 (m, 2H), 8.18 (d, J = 8.0 Hz, 2H), 8.12 (s, 4H), 7.99 (t, J = 8.0 Hz, 1H), 7.83 (s, 2H), 7.71 (br, 2H), 7.52 (br, 1H), 7.45 (br, 1H), 7.24 (d, J = 8.4 Hz, 4H), 6.95 (d, J = 8.4 Hz, 4H), 2.47 (t, J = 7.6 Hz, 4H), 1.55 (s, 36H), 1.25 (m, 22H), 0.84 (m, 8H); ^{13}C NMR ($CDCl_3$, 100 MHz) δ 164.9, 152.5, 152.3, 150.6, 150.3, 150.1, 150.0, 148.6, 143.8, 141.4, 137.3, 137.0, 134.8, 134.5, 133.4, 133.3, 133.1, 131.9, 131.1, 130.8, 130.3, 130.1, 129.6, 129.0, 128.8, 128.7, 128.1, 127.8, 126.8, 126.1, 125.4, 124.5, 124.3, 123.6, 123.5, 122.0, 121.4, 121.3, 120.9, 120.6, 120.5, 108.7, 102.4,

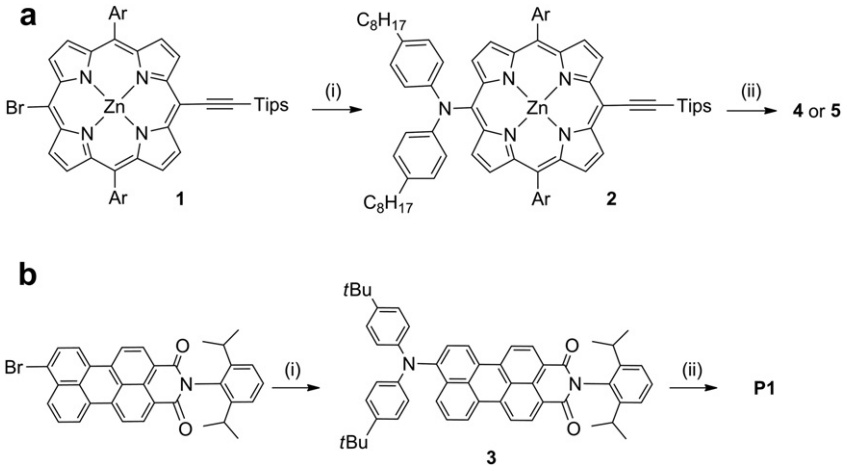

Scheme 1. Synthetic routes for (a) porphyrins **4** and **5**, i) Bis(4-octylphenyl)amine, NaH, $Pd(OAc)_2$, DPEphos, THF. ii) TBAF, THF, RT; then 9-Bromo-3,4-perylenedicarboxylic anhydride for **4** or 4-bromo-1,8-naphthalic anhydride for **5**, [$Pd_2(dba)_3$], $AsPh_3$, THF, NEt_3, reflux; (b) **P1**, i) [$Pd_2(dba)_3$], Di(4-tert-butylphenyl)amine, (*t*-Bu)$_3$P, *t*-BuONa, toluene, reflux. ii) KOH, IPA, reflux.

98.8, 94.4, 35.2, 35.0, 31.8, 31.7, 31.5, 31.2, 29.4, 29.3, 29.2, 22.6, 14.1 UV–Vis (CH_2Cl_2): λ_{max}/nm ($\varepsilon/10^3$ M^{-1} cm^{-1}) = 436(86), 493(50), 548(36), 685(43); IR (KBr, cm^{-1}): ν = 2957, 2924, 2854, 2173, 1707, 1596, 1568, 1506, 1355, 1293, 1244, 800, 715; HRMS: *m*/*z* calcd. for $C_{100}H_{100}N_5O_3Zn$: 1482.7112, found: 1482.6808 ($[M-H]^-$).

2.4.2. Zinc(II) 5,15-Bis(3,5-di-tert-butylphenyl)-10-(bis(4-octylphenyl)amino)-20-(4- (naphthalic-1,8-anhydride)ethynyl) porphyrin (*5*)

Porphyrin **5** was prepared with a procedure similar to that for **4** except 4-bromo-1,8-naphthalic anhydride instead of 9-bromoperylene-3,4-dicarboxylic anhydride. Recrystallization of the product from CH_2Cl_2/CH_3OH gave **5** in a yield 55%. ^1H NMR ($CDCl_3$, 400 MHz) δ 9.77 (d, *J* = 4.4 Hz, 2H), 9.35 (d, *J* = 8.4 Hz, 1H), 9.19 (d, *J* = 4.4 Hz, 2H), 8.97 (d, *J* = 4.4 Hz, 2H), 8.73 (d, *J* = 8.4 Hz, 2H), 8.58 (br, 2H), 8.34 (d, *J* = 5.6 Hz, 1H), 8.00 (s, 4H), 7.96 (t, *J* = 8.0 Hz, 1H), 7.78 (s, 2H), 7.17 (d, *J* = 8.4 Hz, 4H), 6.93 (d, *J* = 8.4 Hz, 4H), 2.47 (t, *J* = 8.0 Hz, 4H), 1.53 (s, 36H), 1.24 (m, 22H), 0.84 (m, 8H); ^{13}C NMR ($CDCl_3$, 100 MHz) δ 158.9, 153.0, 152.1, 150.6, 150.4, 150.2149.0, 141.0, 135.1, 133.7, 132.8, 132.5, 131.4, 130.5, 129.6, 128.9, 128.6, 126.5, 125.8, 124.0, 122.5, 121.2, 117.6, 115.4, 108.7, 105.4, 97.7, 93.1, 35.2, 35.1, 31.7, 31.8, 31.5, 29.7, 29.5, 29.4, 29.2, 22.6, 14.1; UV–Vis (CH_2Cl_2): λ_{max}/nm ($\varepsilon/10^3$ M^{-1} cm^{-1}) = 486(114), 679(38); IR (KBr, cm^{-1}): ν = 2957, 2923, 2854, 2174, 1768, 1719, 1587, 1506, 1451, 1340, 1250, 1018, 800, 711; HRMS: *m*/*z* calcd. for $C_{90}H_{98}N_5O_3Zn$: 1360.6956, found: 1360.6982 ($[M+H]^+$).

2.4.3. N-(2,6-diisopropylphenyl)-9-(bis(4-tert-butylphenyl)amino) perylene-3,4- dicarboximide (*3*)

A mixture of *N*-(2,6-diisopropylphenyl)-9-bromoperylene-3,4-dicarboximide (112 mg, 0.2 mmol), di(4-tert-butylphenyl)amine (112 mg, 0.4 mmol), [$Pd_2(dba)_3$] (10 mg, 0.01 mmol), tri-*tert*-butylphosphine (10 mg, 0.05 mmol), sodium *tert*-butyl alcohol (27 mg, 0.27 mmol) and toluene (50 mL) was heated under reflux under dinitrogen overnight. The solvent was removed under vacuum, and the residue was purified on a column chromatograph (silica gel) using CH_2Cl_2/hexane = 4/6 as eluent. Recrystallization from CH_2Cl_2/CH_3OH gave **3** (126.2 mg, 83%). ^1H NMR ($CDCl_3$, 400 MHz) *δ* 8.67–8.63 (m, 2H), 8.47–8.42 (m, 3H), 8.37 (d, *J* = 8.4 Hz, 1H), 8.08 (d, *J* = 8.4 Hz, 1H), 7.52–7.46 (m, 2H), 7.40 (d, *J* = 8.4 Hz, 1H), 7.34 (d, *J* = 8.0 Hz, 2H), 7.25 (d, *J* = 8.4 Hz, 2H), 7.01 (d, *J* = 8.4 Hz, 2H), 2.78 (m, 2H), 1.31 (s, 18H), 1.18 (d, *J* = 7.2 Hz, 12H);

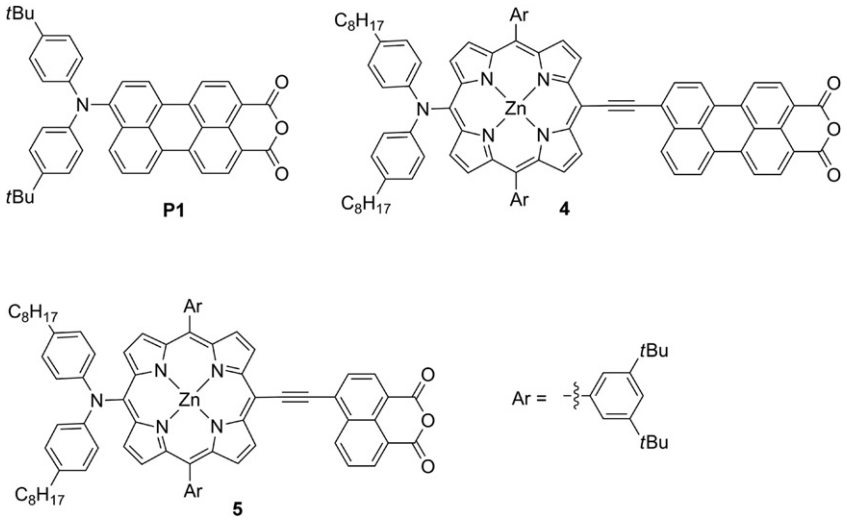

Fig. 1. Molecular structures of dyes **P1**, **4** and **5**.

^{13}C NMR ($CDCl_3$, 100 MHz) δ 164.3, 164.2, 147.8, 146.1, 146.0, 145.8, 138.0, 137.8, 132.4, 132.3, 131.7, 131.4, 130.9, 130.0, 129.9, 129.6, 128.2, 127.4, 127.2, 127.0, 126.4, 125.1, 124.4, 124.2, 122.6, 121.1, 120.5, 120.3, 119.9, 34.5, 31.7, 29.4, 24.3; FAB-MS: *m*/*z* calcd. for $C_{54}H_{52}N_2O_2$: 760; found: 761 ($[M + H]^+$).

2.4.4. 9-(bis(4-tert-butylphenyl)amino)perylene-3,4-dicarboxylic anhydride (*P1*)

A mixture of **3** (164 mg, 0.2 mmol), potassium hydroxide (500 mg, 9 mmol) and isopropanol (50 mL) was heated under reflux with stirring overnight. The reaction mixture was cooled to 23 °C and then poured into acetic acid; the solution was stirred at 23 °C for 6 h. Water was poured into solution and the mixture was filtered. The crude product was washed with water. Column chromatography (silica gel) using CH_2Cl_2/hexane = 8/2 as eluent. Recrystallization from CH_2Cl_2/CH_3OH gave **P1** (108.0 mg, 90%). ^{1}H NMR ($CDCl_3$, 400 MHz) δ 8.37 (d, J = 8.0 Hz, 2H), 8.30 (d, J = 8.0 Hz, 2H), 8.20 (s, J = 8.0 Hz, 1H), 8.15–8.09 (m, 2H), 7.45 (t, J = 8.4 Hz, 1H), 7.35 (d, J = 8.0 Hz, 1H), 7.27 (d, J = 8.4 Hz, 4H), 7.02 (d, J = 8.4 Hz, 4H), 1.31 (s, 18H); ^{13}C NMR ($CDCl_3$, 100 MHz) δ 160.4, 160.3, 148.4, 145.6, 145.5, 138.5, 138.4, 133.1, 132.9, 132.1, 130.7, 129.4, 128.6, 128.5, 126.6, 126.5, 126.1, 125.9, 125.3, 124.7, 124.4, 122.4, 119.6, 119.2, 116.0, 115.2, 34.0, 31.1; UV–vis (CH_2Cl_2): λ_{max}/nm (ε/10^3 M^{-1} cm^{-1}) = 486(9), 593(20); IR (KBr, cm^{-1}): ν = 2958, 2868, 1699, 1664, 1567, 1499, 1356, 1266, 1100, 1018, 813, 755; HRMS: *m*/*z* calcd. for $C_{42}H_{35}NO_3$: 601.2611, found: 601.2590 ($[M]^-$).

3. Results and discussion

The absorption spectrum of a porphyrin dye generally features an intense Soret band in the range 400–450 nm and less intense Q bands in the range 550–650 nm. The gap between 450 and 550 nm is amenable to structural modification, such that the absorption position and width can be tuned in a controllable fashion. To be an efficient dye, an objective would be for the dye to absorb intensely across the entire visible region, even extending into the near-IR region. The existence of that absorption gap between the Soret and Q bands decreases the light-harvesting efficiency of a porphyrin. The spectral characteristics of perylene dyes that typically have absorption bands in the range 450–550 nm make them ideal auxiliary pigments for combination with porphyrins to improve the light-harvesting efficiency. As mentioned, an extension of π-conjugation in porphyrin would lead to broadening and red shift of the absorption bands. We therefore designed a dyad **4** with a perylene anhydride connected to the porphyrin via an acetylenic link; the highly conjugated acetylenic bridge would efficiently mediate electronic interaction between the porphyrin and perylene units. The synthesis of porphyrin-based dyads involved a Sonogashira coupling reaction between ethynylporphyrin and the appropriate bromide. As shown in Scheme 1, deprotection of porphyrin **2** [5] followed by coupling to perylene bromide using Pd as catalyst gave dyad **4**. Porphyrin **5** was similarly synthesized; these molecular structures are shown in Fig. 1.

Table 1
Spectral and electrochemical data for **P1**, **2**, **4**, and **5** dyes.[a]

Dye[a]	Absorption λ_{max}/nm (ε/10^3 M^{-1} cm^{-1})	Emission λ_{max}/nm (ϕ)[b]	Oxidation $E_{1/2}$/V	Reduction $E_{1/2}$/V
2	428(233), 574(12), 634(27)	677 (0.0548)	+0.92, +1.32[c]	−1.11
P1	486(9), 593(20)	604, 743 (0.0404)	+1.23	−0.71, −1.29
4	436(86), 493(50), 548(36), 685(43)	787 (0.0006)	+0.92, +1.29[c]	−0.72, −0.93, −1.47
5	440(114), 679(38)	738 (0.0267)	+0.94, +1.32[c]	−0.81. −1.00

[a] Absorption and emission data were measured in CH_2Cl_2 at 25 °C. Electrochemical measurements were performed at 25 °C in THF containing $TBAPF_6$ (0.1 M) as supporting electrolyte. Potentials measured *vs*. ferrocene/ferrocenium (Fc/Fc^+) couple were converted to normal hydrogen electrode (NHE) by addition of +0.63 V.
[b] The excitation wavelengths were 570, 650 and 620 nm for **P1**, **4** and **5**, respectively. ZnTPP was used as the reference for the calculation of quantum yields.
[c] Irreversible process E*pa* or E*pc*.

Reference compound **P1** shows a visible spectrum with absorption maxima at 486 (ε = 9000 M^{-1} cm^{-1}) and 593 nm (ε = 20 000 M^{-1} cm^{-1}). The absorption spectrum of dyad **4** differs much from the combined spectrum of the respective porphyrin and perylene components. As shown in Fig. 2, porphyrin **4** shows broad absorption bands that cover almost the entire visible region and extend into the near-IR region; the absorption gap between the Soret and Q bands is filled through the absorption of the perylene unit. As expected, an attachment of the perylene to the porphyrin via the carbon–carbon triple bond significantly perturbs the photophysical properties of the perylene and the porphyrin. Both the Soret and Q bands of **4** show a significant red shift, indicating a decreased energy gap between the HOMO and the LUMO as a consequence of extension of π-conjugation [26]. Furthermore, compound **4** exhibits broadening of the Soret band, indicating a strong electronic coupling between the porphyrin and perylene units. The band broadening and red shifts for **5** are less than for **4** because the electronic interaction with the porphyrin is more pronounced for the perylene than for the naphthalene. Dyads **4** and **5** notably exhibit significantly intensified Q bands through the energy splitting between the a_{1u} and a_{2u} orbitals, or the e_g orbitals [26]. Such enhanced absorption would enhance the light-harvesting efficiency and is thus expected to enable the use of thinner films to fabricate the devices. This condition might increase the open circuit voltage and the overall efficiency of power conversion, and prevent a decreased mechanical strength of the film [27].

The emission data for dyes **P1**, **4**, **5**, and the component subunit **2** in CH_2Cl_2 at 23 °C are listed in Table 1. The emission of porphyrin **2**

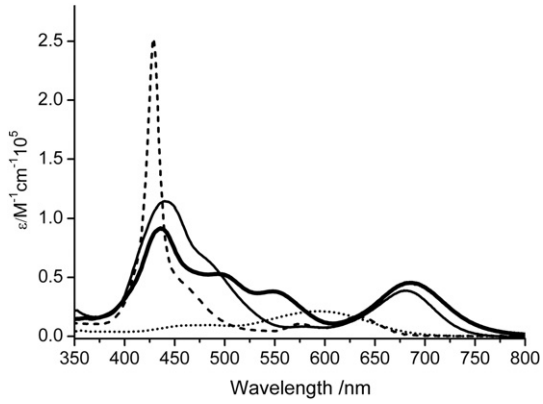

Fig. 2. Absorption spectra of porphyrins **4** (plain), **5** (bold), **2** (dash), and **P1** (dot).

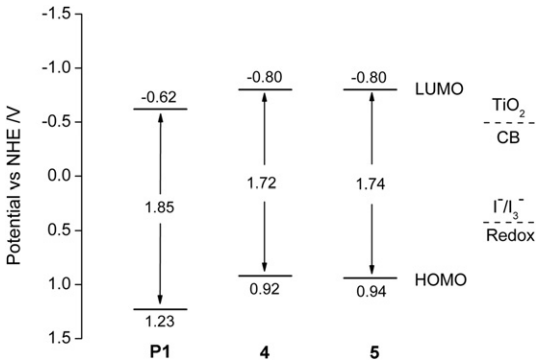

Fig. 3. Energy levels of **P1**, **4** and **5**.

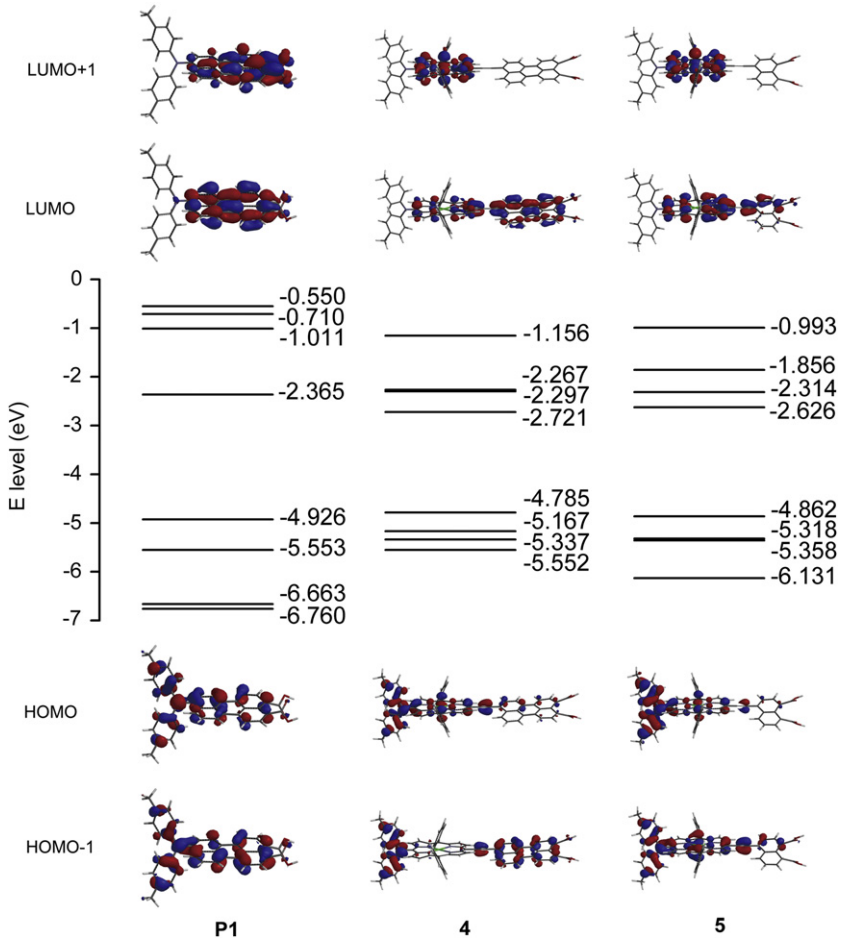

Fig. 4. HOMO − 1, HOMO, LUMO and LUMO + 1 for dicarboxylic acids of **P1**, **4** and **5** in the gaseous phase.

is dominated by the Q band at 673 nm. In the case of dyads **4** and **5**, the emission was observed in the range 700–800 nm. The significant red shift is consistent with the elongation of π-conjugation, but the emission intensity of **4** and **5** is decreased. This result might be diagnostic of efficient transfer of energy or electrons from the excited porphyrin to the acceptor element in the dyads.

Appropriate HOMO and LUMO energy levels of the dye are required to match the oxidation potential of the I^-/I_3^- electrolyte and the conduction-band (CB) edge level of the TiO_2 electrode. Electrochemical tests were performed to determine the HOMO levels of the dyes, which correspond to the first oxidation potentials of the sensitizers. The cyclic voltammetry measurements for **P1**, **4** and **5** in CH_2Cl_2 were conducted using tetrabutylammonium hexafluorophosphate ($TBAPF_6$, 0.1 M) as supporting electrolyte; the potentials are listed in Table 1. Perylene **P1** shows reversible oxidation at $E_{1/2} = +1.23$. The first oxidations for **4** and **5**, which are reversible, appear at $E_{1/2} = +0.92$ and $+0.94$ V, respectively, whereas the second oxidations are irreversible and occur at $E_{pa} = +1.32$ and $+1.29$ V. As shown in Fig. 3, the excited-state oxidation potentials ($E^*_{0\text{-}0}$) of **P1**, **4** and **5** are −0.62, −0.80 and −0.80 V, respectively, as calculated from the oxidation potential (E_{ox}) and the optical band gap ($E_{0\text{-}0}$) determined from the intersection of the corresponding absorption and emission spectra. The $E^*_{0\text{-}0}$ values for these dyes are more negative than the conduction-band level of TiO_2 (∼−0.5 V versus NHE) ensuring a sufficient driving force for electron injection.

To acquire insight into the electronic distribution at the frontier and close-lying molecular orbitals, we performed quantum-chemical calculations on these dyes using density-functional theory (DFT) at the B3LYP/6-31G(d) level (Spartan 08 package). To simplify the computations, some alkyl groups on phenyl rings were replaced with hydrogen atoms or methyl groups. Fig. 4 shows an energy-level diagram and the corresponding molecular orbitals for these porphyrin dyes. The electronic distribution of HOMO and HOMO − 1 for **P1** is delocalized over both diarylamine and perylene units whereas that of LUMO and LUMO + 1 is localized on the perylene. At the HOMO level of **4** and **5**, the electronic density is distributed mainly on the diarylamine and porphyrin. The distribution of electronic density of the LUMO is located primarily at the porphyrin, and the perylene or naphthalene unit. Comparison of **4** with **5** shows that the HOMO–LUMO gap is decreased upon extension of π-conjugation because considerable electronic coupling occurs between the link and the porphyrin core. This effect is in agreement with the more pronounced red shift and broadening in the absorption bands for **4** than **5**. The electronic distributions of the frontier orbitals indicate that these dyes are suitable for use in DSSC devices.

The perylene **P1** and porphyrins **4** and **5** were sensitized onto TiO_2 nanoparticulate films to serve as working electrodes of DSSC devices for photovoltaic characterization. Fig. 5a presents absorption spectra of the sensitized samples as thin films and Fig. 5b shows the corresponding IPCE action spectra of the devices. Fig. 5c shows the current-voltage characteristics of these three dyes on TiO_2 films of thickness 10 μm under the same conditions of device fabrication; the corresponding photovoltaic parameters are summarized in Table 2. The Soret bands of **4** and **5** adsorbed on TiO_2 films show a saturated feature but the Q bands are significantly

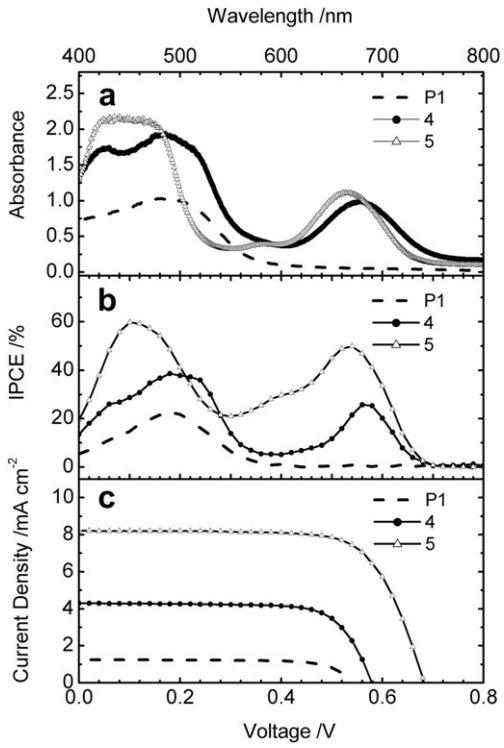

Fig. 5. (a) Absorption spectra of films, (b) IPCE action spectra of devices, and (c) current-voltage characteristics of devices fabricated with **P1**, **4** and **5** sensitized on TiO_2 films.

blue-shifted with respect to those shown in solution (Fig. 2). This blue-shifted feature was more pronounced for **P1**, indicating that $\pi-\pi$ stacking of the dye on TiO_2 was in an H-type manner. The IPCE spectra show a systematic trend **5** > **4** > **P1**, which is consistent with the variation of J_{SC} showing the same order (**5** > **4** > **P1**). The overall efficiencies of **P1**, **4** and **5** are 0.5, 1.8 and 3.9%, respectively, for an immersion period 4 h. The amounts of dye-loading are determined to be 184, 119 and 143 nmol cm^{-2} for **P1**, **4** and **5**, respectively. When the immersion period was increased to 8 h, the efficiencies of **P1**, **4** and **5** decreased to 0.3, 1.1 and 3.7%, respectively. Even though the amounts of dye-loading increased with increasing immersion period, the corresponding cell performances decreased. In particular, **4** shows a decrease in cell performance of ca. 40% when the immersion period was increased from 4 h to 8 h. Because of the planar feature of the molecule, we expect that dye aggregation was a major problem for the poor performance of **4**. On the other hand, the extent of dye aggregation for **5** is less significant. We have shown that aggregation of porphyrin dyes on TiO_2 surface results in rapid intermolecular energy transfer that substantially reduces the efficiency of electron injection and leads to poor cell performance [28,29]. Even though less dye molecules were adsorbed on the TiO_2 film, **5** showed much better cell performance over that of **4**. To design a new dye based on the structure of **5**, one should consider a structural modification that results in the filling of the IPCE spectral gap between Soret and Q bands and to further reduce dye aggregation so as to reach higher value of J_{SC} for better cell performance.

Table 2
Photovoltaic parameters of DSSC made of **P1**, **4** and **5** with TiO_2 film (thickness 10 μm) under simulated illumination (AM1.5, power 100 mW cm^{-2}) and active area 0.16 cm^2.

Dye	J_{sc}/mA cm^{-2}	V_{oc}/V	FF	η%
P1	1.23	0.545	0.74	0.5
4	4.28	0.582	0.71	1.8
5	8.26	0.684	0.69	3.9

4. Conclusion

Two novel electronically coupled porphyrin-arene dyads **4** and **5** have been synthesized and applied in dye-sensitized solar cells. A perylene sensitizer **P1** was synthesized and tested for comparison. As a consequence of an extended π-conjugation, both Soret and Q bands of **4** exhibit a significant red shift and a Soret band broader than that of **5**, because the electronic interaction with the porphyrin is more pronounced for the perylene than for the naphthalene. The results clearly show that π-conjugation with a highly conjugated acetylenic bridge unit can improve the light-harvesting capability of porphyrin dyes. Of the two porphyrin dyes, **5** exhibits a greater efficiency of power conversion, 3.9%, which is 7.8 times the value for **P1** under similar conditions. The IPCE spectra and J_{SC} shows a trend for **5** > **4** > **P1**. The overall efficiencies of **P1**, **4** and **5** for immersion periods 4 and 8 h are 0.5, 1.8 and 3.9%, and 0.3, 1.1 and 3.7% respectively. The poor photovoltaic performance of dye **4** is due to the formation of aggregates. To improve the performance of solar cells, further structural modification of the *meso*-substituted porphyrins to suppress dye aggregation is under investigation in our laboratory.

Acknowledgement

National Science Council of Taiwan and Ministry of Education of Taiwan, R.O.C., under the ATU program, provided support for this project.

Appendix. Supplementary data

Supplementary data associated with this article can be found in the online version, at doi:10.1016/j.dyepig.2011.04.010.

References

[1] Deisenhofer J, Norris JR, editors. The photosynthetic reaction. New York USA: Academic Press; 1993.
[2] Tani F, Matsu-ura M, Nakayama S, Naruta Y. Synthetic models for the active site of cytochrome P450. Coordination Chemistry Reviews 2002;226:219.
[3] Colluman JP, Wang Z, Straumanis A, Quelquejeu M. An efficient catalyst for asymmetric epoxidation of terminal olefins. Journal of American Chemical Society 1999;121:460–1.
[4] Kessel D, Dougherty TJ, Chang CK. Photosensitization by synthetic diporphyrins and dichlorins in vivo and in vitro. Photochemistry and Photobiology 1991;53:475–9.
[5] Lee CW, Lu HP, Lan CM, Liang YR, Yen WN, Liu YC, et al. Novel zinc porphyrin sensitizers for dye-sensitized solar cells: synthesis and spectral, electrochemical, and photovoltaic properties. Chemistry – A European Journal 2009; 15:1403–12.
[6] Takahashi K, Iwanaga T, Yamaguchi T, Komura T, Murata K. Porphyrin dye-sensitization of polythiophene in a conjugated polymer/TiO_2 p-n heterojunction solar cell. Synthetic Metals 2001;123:91–4.
[7] Hasobe T, Kamat PV, Absalom MA, Kashiwagi Y, Sly J, Crossley MJ, et al. Supramolecular photovoltaic cells based on composite molecular nanoclusters: dendritic porphyrin and C_{60}, porphyrin dimer and C_{60}, and porphyrin–C_{60} dyad. Journal of Physical Chemistry B 2004;108:12865–72.
[8] Huijser A, Savenije TJ, Kroeze JE, Siebbeles LDA. Exciton diffusion and interfacial charge separation in meso-tetraphenylporphyrin/TiO_2 bilayers: effect of ethyl substituents. Journal of Physical Chemistry B 2005;109:20166–73.
[9] Huijser A, Marek PL, Savenije TJ, Siebbeles LDA, Scherer T, Hauschild R, et al. Photosensitization of TiO_2 and SnO_2 by artificial self-assembling mimics of the natural chlorosomal bacteriochlorophylls. Journal of Physical Chemistry C 2007;111:11726–33.
[10] Campbell WM, Jolley KW, Wagner P, Wagner K, Walsh PJ, Gordon KC, et al. Highly efficient porphyrin sensitizers for dye-sensitized solar cells. Journal of Physical Chemistry C 2007;111:11760–2.

[11] Ventura B, Flamigni L, Marconi G, Lodato F, Officer DL. Extending the porphyrin core: synthesis and photophysical characterization of porphyrins with π-conjugated β-substituents. New Journal of Chemistry 2008;32:166–78.
[12] Eu S, Hayashi S, Umeyama T, Matano Y, Araki Y, Imahori H. Quinoxaline-fused porphyrins for dye-sensitized solar cells. Journal of Physical Chemistry C 2008;112:4396–405.
[13] Martinez-Díaz MV, de la Torre G, Torres T. Lighting porphyrins and phthalocyanines for molecular photovoltaics. Chemical Communications 2010;46:7090–108.
[14] Imahori H, Umeyama T, Ito S. Large π-aromatic molecules as potential sensitizers for highly efficient dye-sensitized solar cells. Accounts of Chemical Research 2009;42:1809–18.
[15] Waltera MG, Rudineb AB, Wamser CC. Porphyrins and phthalocyanines in solar photovoltaic cells. Journal of Porphyrins and Phthalocyanines 2010;14:759–92.
[16] Wang Q, Ito S, Grätzel M, Fabregat-Santiago F, Mora-Seró I, Bisquert J, et al. Characteristics of highly efficient dye-sensitized solar cells. Journal of Physical Chemistry B 2006;110:25210–21.
[17] Gao F, Wang Y, Shi D, Zhang J, Wang M, Jing X, et al. Enhance the optical absorptivity of nanocrystalline TiO_2 film with high molar extinction coefficient ruthenium sensitizers for high performance dye-sensitized solar cells. Journal of American Chemical Society 2008;130:10720–8.
[18] Nazeeruddin MK, Humphry-Baker R, Officer DL, Campbell WM, Burrell AK, Grätzel M. Application of metalloporphyrins in nanocrystalline dye-sensitized solar cells for conversion of sunlight into electricity. Langmuir 2004;20:6514–7.
[19] Hayashi S, Tanaka M, Hayashi H, Eu S, Umeyama T, Matano Y, et al. Naphthyl-fused π-elongated porphyrins for dye-sensitized TiO_2 cells. Journal of Physical Chemistry C 2008;112:15576–85.
[20] Jacob J, Sax S, Piok T, List EJW, Grimsdale AC, Müllen K. Ladder-type pentaphenylenes and their polymers: efficient blue-light emitters and electron-accepting materials via a common intermediate. Journal of American Chemical Society 2004;126:6987–95.
[21] Lemaur V, Steel M, Beljonne D, Brédas JL, Cornil J. Photoinduced charge generation and recombination dynamics in model donor/acceptor pairs for organic solar cell applications: a full quantum-chemical treatment. Journal of American Chemical Society 2005;127:6077–86.
[22] Neuteboom EE, Meskers SCJ, Van Hal PA, Van Duren JKJ, Meijer EW, Janssen RAJ, et al. Alternating oligo(*p*-phenylene vinylene)–perylene bisimide copolymers: synthesis, photophysics, and photovoltaic properties of a new class of donor–acceptor materials. Journal of American Chemical Society 2003;125:8625–38.
[23] Schmidt-Mende L, Fechtenkotter A, Müllen K, Moons E, Friend RH, MacKenzie JD. Self-organized discotic liquid crystals for high-efficiency organic photovoltaics. Science 2001;293:1119–22.
[24] Edvinsson T, Li C, Pschirer N, Schöneboom J, Eickemeyer F, Sens R, et al. Intramolecular charge-transfer tuning of perylenes: spectroscopic features and performance in dye-sensitized solar cells. Journal of Physical Chemistry C 2007;111:15137–40.
[25] Li C, Yum JH, Moon SJ, Herrmann A, Eickemeyer F, Pschirer NG, et al. An improved perylene sensitizer for solar cell applications. ChemSusChem 2008;1:615–8.
[26] Anderson HL. Building molecular wires from the colours of life: conjugated porphyrin oligomers. Chemical Communications; 1999:2323–30.
[27] Choi H, Raabe I, Kim D, Teocoli F, Kim C, Song K, et al. High molar extinction coefficient organic sensitizers for efficient dye-sensitized solar cells. Chemistry – A European Journal 2010;16:1193–201.
[28] Luo L, Lin CJ, Tsai CY, Wu HP, Li LL, Lo CF, et al. Effects of aggregation and electron injection on photovoltaic performance of porphyrin-based solar cells with ligo(phenylethynyl) links inside TiO_2 and Al_2O_3 nanotube arrays. Physical Chemistry Chemical Physics 2010;12:1064–71.
[29] Luo L, Lin CJ, Hung CS, Lo CF, Lin CY, Diau EWG. Effects of potential shift and efficiency of charge collection on nanotube-based porphyrin-sensitized solar cells with conjugated links of varied length. Physical Chemistry Chemical Physics 2010;12:12973–7.